

Numerical simulation of the effect of the free carrier motilities on light-soaked a-Si:H p-i-n solar cell

L. Ayat¹, A. F. Bouhdjar², AF. Meftah^{2,†}, and N. Sengouga²

¹Laboratory of Semiconductor Devices Physics, Physics Department, University of Béchar, P. O. Box 417, Béchar 08000, Algeria

²Faculté des Sciences de la matière, Laboratoire des Matériaux Semi-conducteurs et Métalliques, Université Mohammed Khider, B. P. 145, Biskra 07000, Algérie

Abstract: Using a previous model, which was developed to describe the light-induced creation of the defect density in the a-Si:H gap states, we present in this work a computer simulation of the a-Si:H p-i-n solar cell behavior under continuous illumination. We have considered the simple case of a monochromatic light beam nonuniformly absorbed. As a consequence of this light-absorption profile, the increase of the dangling bond density is assumed to be inhomogeneous over the intrinsic layer (i-layer). We investigate the internal variable profiles during illumination to understand in more detail the changes resulting from the light-induced degradation effect. Changes in the cell external parameters including the open circuit voltage, V_{oc} , the short circuit current density, J_{sc} , the fill factor, FF, and the maximum power density, P_{max} , are also presented. This shows, in addition, the free carrier mobility influence. The obtained results show that V_{oc} seems to be the less affected parameter by the light-induced increase of the dangling bond density. Moreover, its degradation is very weak-sensitive to the free carrier mobility. Finally, the free hole mobility effect is found to be more important than that of electrons in the improvement of the solar cell performance.

Key words: a-Si:H; Staebler-Wronski effect; defect pool model; p-i-n

DOI: 10.1088/1674-4926/36/7/074002

EEACC: 2520

1. Introduction

As is well known, the degradation of transport proprieties during illumination of the hydrogenated amorphous silicon (a-Si:H) materials, i.e., the so-called Staebler–Wronski effect (SWE)^[1], is the main problem limiting the applicability of such materials in photovoltaic domains. This effect presents a challenge to physics and engineering of a-Si:H solar cells. The recombination of free carrier excess created by illumination causes the formation of new dangling bonds, i.e., of additional recombination centres^[2], which affects the lifetime of carriers. Then, the SWE affects the performance of the a-Si:H solar cell; its photo-parameters decrease under illumination. Since this is a self-limiting process^[2], the cell's photo-parameters stabilize after a certain time at values below the initials one.

The increase of the dangling bond density of state distribution in the a-Si:H gap during illumination is obtained on the basis of our model of the light-induced defect creation in a-Si:H^[3,4]. The proposed model is based on experimental observation concerning the presence of the SiHHSi configuration^[5,6], the hydrogen diffusion^[7] and the main role of the hydrogen in the light-induced defect annealing^[8–12]. The varying density of states is then used in the numerical modelling of the a-Si:H p-i-n solar cell, illuminated with monochromatic light beam. This considers the case of non uniform absorption, which means an exponential decrease in the generation rate from the illuminated p-side to the n-side of the device. Consequently, we assume an inhomogeneous light-induced increase of the dangling bond density of state distribution over

the i-layer. We analyze the degradation in terms of the internal variable profiles: free carriers, recombination rates, space charges, band structure, electric field, and current densities. We present also the light-induced degradation effect on the cell photo-parameter, i.e. the open circuit voltage V_{oc} , the short circuit current density J_{sc} , the fill factor FF and the maximum power density P_{max} , and the influence of the free electron and hole mobilities on the degradation process of these parameters.

2. The SWE model

The basic processes for light-induced creation of dangling bonds in our model^[3,4] are given as follows: the defect creation occurs by a non radiative recombination between photoexcited electrons and holes at a weak Si–Si bond adjacent to a doubly hydrogenated weak Si–Si bond, SiHHSi. This can be justified by the fact that the majority of hydrogen is located in SiHHSi configurations rather than in isolated Si–H bonds^[5]. This weak Si–Si bond is energetically favourable for recombination due to the additional stress imposed by the two hydrogen atoms. After recombination and the resulting energy release, one of the two hydrogen atoms moves to the site of the broken Si–Si bond, forming two adjoining SiHD defects. The hydrogen atom is located at the tetrahedral site, rather than at the bond centred site, of the broken Si–Si bond, and the separation of the Si dangling bond and hydrogen atom is in the range 4–5 Å, which is consistent with ESR experiments^[5]. The recombination at the SiHD defect site allows the production and diffusion of a mobile hydrogen atom through the material. If the dissoci-

† Corresponding author. Email: af_mef@yahoo.fr
Received 15 July 2014

ated hydrogen atom is inserted in the nearby SiHD defect, this will be annihilated and, in this case there will be no defect creation and no SWE as a consequence. Thus, the hydrogen atom remains mobile until it meets a distant SiHD defect where they annihilate to form a SiHHSi bond. The hydrogen atom can also be re-trapped by colliding with a second metastable H. In this case, both metastable Hs are trapped to form a SiHHSi bond again. Taking into account the processes described above, the rate equations governing the kinetics of SiHD and metastable H under illumination are given as follows:

$$\frac{dN_d}{dt} = R_{SiSi} - R_{SiHD} - C_d^c N_H N_d, \quad (1)$$

$$\frac{dN_H}{dt} = R_{SiHD} - C_d^c N_H N_d - 2C_H^c N_H^2, \quad (2)$$

where N_d and N_H are densities of SiHD and metastable H, respectively. $R_{SiSi} = k_d n p$, where k_d expresses the light-induced creation of SiHD. n and p are the free electron and free hole densities. $R_{SiHD} = k_H n p$, where k_H represents dissociation of a hydrogen atom from a SiHD defect. C_d^c and C_H^c are rate constants for the two trapping processes of the hydrogen atom. We assume that n and p are determined by the steady state numbers and are, in the case of moderate illumination where the recombination is monomolecular, proportional to illumination intensity G and inversely proportional to the defect density N_d :

$$n = p = \frac{G}{C_c N_d}, \quad (3)$$

where C_c (10^{-8} cm³/s) is the capture coefficient of free carriers by dangling bonds. Then, the rate equations 1 and 2 are rewritten as follows:

$$\frac{dN_d}{dt} = \frac{k_d G^2}{C_c^2 N_d^2} - \frac{k_H G^2}{C_c^2 N_d^2} - C_d^c N_H N_d, \quad (4)$$

$$\frac{dN_H}{dt} = \frac{k_H G^2}{C_c^2 N_d^2} - C_d^c N_H N_d - 2C_H^c N_H^2. \quad (5)$$

The initial conditions are $N_d = 10^{16}$ cm⁻³ and $N_H = 0$ and the values of the different involved constants are those used previously in References [3, 4] which reproduced well Godet's measurement: $k_d = 5 \times 10^{-15}$ cm³/s, $k_H = 3 \times 10^{-15}$ cm³/s, $C_d^c = 4 \times 10^{-19}$ cm³/s and $C_H^c = 10^{-17}$ cm³/s. From the simulated curve shown in Figure 1, the dangling bond (SiHD) density increases from 10^{16} cm⁻³ initially to a steady state value of 3.75×10^{16} cm⁻³ for illumination time $> 10^4$ s. The metastable hydrogen increases nearly exponentially until 40 s what delays the increase of the SiHD density. After 40 s, the decrease of the metastable hydrogen occurs parallel to the inverse of the SiHD density until 2×10^4 s, after which a steady state is established for the two densities.

3. Evolution of the density of states with illumination time

The typical density of localised states, $g(E)$, in the a-Si:H gap is comprised of the band tail state density, which decays exponentially from the band edge, and of the dangling bond state density. The latter is calculated according to the defect pool model improved by Powell and Deane^[13].

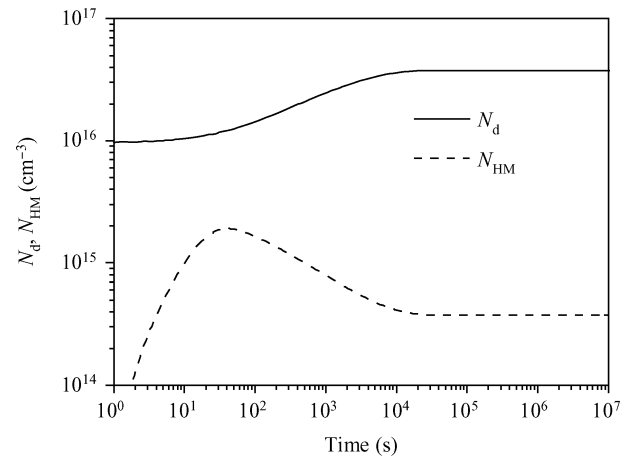


Figure 1. Simulation of the light-induced defect and mobile hydrogen creation following the proposed model^[3, 4].

The defect pool model, proposed for the equilibrium properties of a-Si:H, can account for a wide range of experimental results^[13, 14]. The equilibration mechanism was identified as a conversion of weak bond to dangling bond according to the reaction: SiHHSi + SiSi \leftrightarrow 2SiHD^[13]. The density of state distribution was determined by applying the law of mass action to both reactions: SiHD \leftrightarrow SiSi + H and SiHHSi \leftrightarrow SiSi + 2H between weak bond energy in the valence band tail and energy level in the gap where the defect is formed. The density of state calculated within the framework of the defect pool model is expressed as follows^[13]:

$$D(E) = \gamma \left[\frac{2}{f^o(E)} \right]^{K_B T^*/2E_{v0}} P \left[E + \frac{\sigma^2}{2E_{v0}} \right], \quad (6)$$

with

$$\gamma = \left[\frac{G_v 2E_{v0}^2}{(2E_{v0} - K_B T^*)} \right] \left[\frac{H}{N_{SiSi}} \right]^{K_B T^*/4E_{v0}} \times \exp \left[\frac{-1}{2E_{v0}} \left(E_p - E_v - \frac{\sigma^2}{4E_{v0}} \right) \right],$$

$P(E)$ is the defect pool function assumed to have a Gaussian distribution. σ and E_p are, respectively, the pool width and peak position. G_v and E_{v0} are, respectively, the density of states at E_v and the valence band tail width. T^* is the equilibrium temperature (freeze-in temperature) for which the density of states is maintained. H is the total hydrogen concentration and N_{SiSi} is the total electron concentration in the material. $f^o(E)$ is the neutral dangling bond state occupancy. Schmidt *et al.*^[15, 16] have studied the light-induced degradation of an a-Si:H sample by the constant photocurrent method. They have found that density of occupied states obtained from the deconvolution procedure shows the presence of two peaks within the gap, which are fitted with two Gaussians ascribed to the neutral and negatively charged dangling bonds. The areas of both Gaussians increase as $t^{1/3}$ while their positions and widths remain unchanged on the illumination time. The valence band tail is also found to be practically constant on the illumination time. These observations allow us to propose the following features for the density of states during illumination:

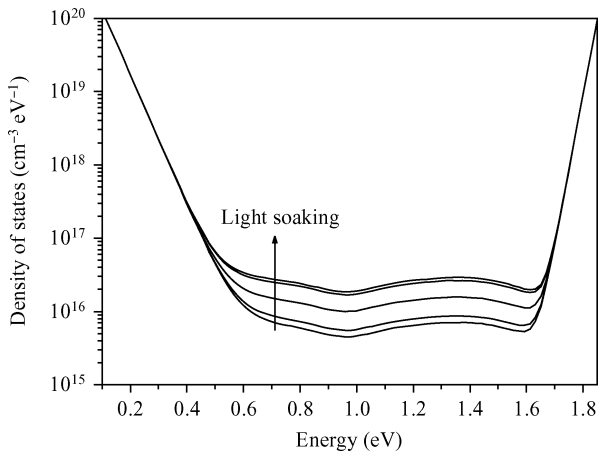


Figure 2. Light-induced increase of the defect state density in the gap of the a-Si:H.

Table 1. Density of states parameters.

Parameter	Value	Parameter	Value
σ	0.19 eV	G_c, G_v	$10^{21} \text{ cm}^{-3} \text{ eV}^{-1}$
E_p	1.27 eV	H	$5 \times 10^{21} \text{ cm}^{-3}$
T^*	500 K	N_{SiSi}	$2 \times 10^{23} \text{ cm}^{-3}$
T_c	246 K	E_{Fi}	0.98 eV
T_v	570 K	$E_c - E_v$	1.9 eV

- (1) The pool width and peak position remain unchanged.
- (2) The pool area increases by the same evolution factor of the defect density, $N_d(t)$.
- (3) The conduction and the valence band tails remain unchanged.

Figure 2 shows the evolution of the defect state density with illumination time taking into account the assumptions above. Parameters used for the defect state density calculation are given in Table 1. Later, we will implant this density of states, varying with illumination time, in the numerical modelling of the a-Si:H p-i-n solar cell to analyze the related degradation effect on the internal variables and the photo-parameters of the cell.

4. Numerical model of the a-Si:H p-i-n cell

The numerical modelling of the a-Si:H p-i-n solar cell, taken as a one-dimensional device, requires the simultaneous resolution of the complete set of transport equations: the electron and hole continuity equations:

$$\frac{1}{q} \frac{dJ_n}{dx} + G(x) - U_r(x) = 0, \quad (7)$$

$$\frac{1}{q} \frac{dJ_p}{dx} - G(x) + U_r(x) = 0, \quad (8)$$

and Poisson's equation:

$$\frac{d^2\psi}{dx^2} = -\frac{q}{\epsilon\epsilon_0} \rho(x), \quad (9)$$

where

$$J_n = -q\mu_n n \frac{d\psi}{dx} + k_B T \mu_n \frac{dn}{dx}, \quad (10)$$

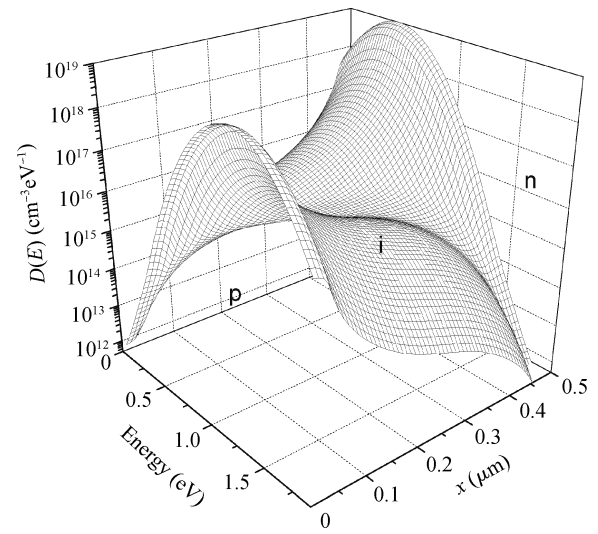


Figure 3. 3D variation of the defect state density.

and

$$J_p = -q\mu_p p \frac{d\psi}{dx} - k_B T \mu_p \frac{dp}{dx}, \quad (11)$$

are the electron and hole conduction current densities, x is the space coordinate, G is the generation rate, μ_n and μ_p are the electron and hole band mobilities, T is the absolute temperature, $\epsilon_0 = 8.85 \times 10^{-14} \text{ F/cm}$ the permittivity of the free space, ϵ the dielectric constant and k_B is the Boltzmann constant. The space charge density $\rho(x)$ and the recombination rate $U_r(x)$ depend on the free electron and hole concentrations, n and p , as well as on the distribution of localised states, $g(E)$, described above.

We take into account the spatial distribution of the dangling bond density of states, $D(E)$, resulting from the spatial variation of the Fermi-level position within the energy gap. The obtained 3-D variation of $D(E)$ at thermal equilibrium is shown in Figure 3. Here, thicknesses of the p and n layers are both $0.01 \mu\text{m}$ and the whole device thickness is $0.5 \mu\text{m}$. To account for the transmittance T of the glass/TCO substrate and the back reflection of the n /metal contact, the generation rate G distribution is given by the following expression:

$$G(x) = T\alpha\phi \{ \exp(-\alpha x) + R \exp[-\alpha(2d - x)] \}, \quad (12)$$

where α is the absorption coefficient, ϕ is the photon flux, and d the thickness of the device.

To solve the set of coupled differential equations we have assumed that the contacts act as neutral contacts; i.e., equilibrium boundary conditions. The numerical resolution method used here is identical to the one described in Reference [17] using the simulation parameters listed in Table 2.

5. Results

The knowledge about the distribution of internal variables is important for understanding the changes resulting from the light-induced degradation in the p-i-n device. To simulate cell behaviour under the light-soaked condition, the dangling bond density of states in the intrinsic layer (i-layer) had to be raised using our model of the light-induced defect increase in the gap

Table 2. Simulation parameters of the a-Si:H p-i-n cell. C_{nt} , C_{ct} , C_{nd} and C_{cd} , are the capture coefficients of the neutral and charged states in band tails and dangling bonds, respectively. N_a and N_d are, respectively, the p- and n-layer doping densities.

$\epsilon\epsilon_0 = 1.0536 \times 10^{-12}$ F/cm	$C_{nc} = C_{pv} = C_{nt} = 10^{-8}$ cm ³ /s
$T = 300$ K	$C_{nv} = C_{pc} = C_{ct} = 10^{-7}$ cm ³ /s
$\mu_n = 20$ cm ² /(V·s)	$C_n^+ = C_p^- = C_{cd} = 10^{-7}$ cm ³ /s
$\mu_p = 2$ cm ² /(V·s)	$C_n^0 = C_p^0 = C_{nd} = 10^{-8}$ cm ³ /s
$N_a = 5 \times 10^{18}$ cm ⁻³	$E_{ip} - E_v = 0.28$ eV
$N_d = 5 \times 10^{18}$ cm ⁻³	$E_c - E_{fn} = 0.24$ eV
T (Transmittance) = 0.9	$\phi = 10^{17}$ cm ⁻² s ⁻¹
R (Back reflection) = 0.9	$\alpha = 10^5$ cm ⁻¹

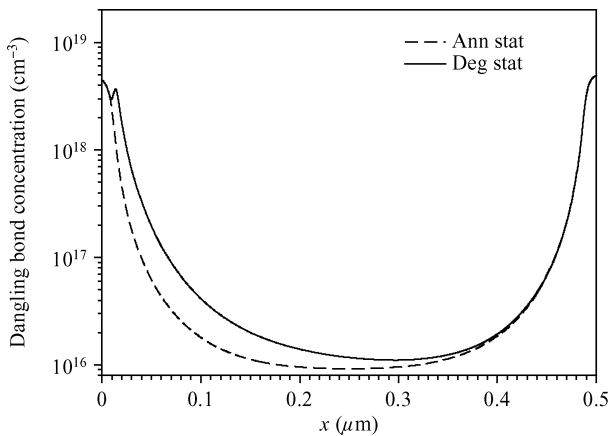


Figure 4. Dangling bond concentration profiles.

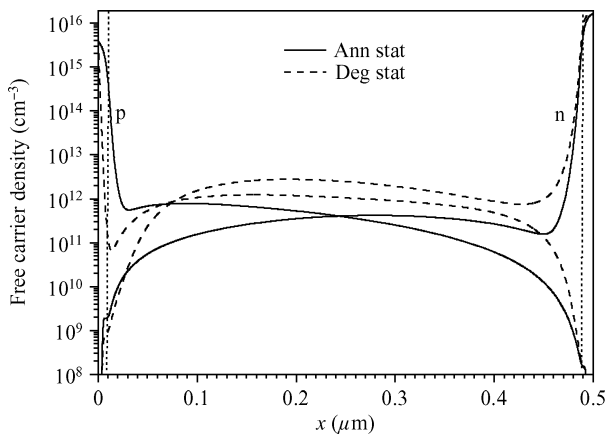


Figure 5. n and p density profiles, under short circuit condition.

states. Since the dangling bond state density is our mean to reproduce the degradation phenomenon, we begin by illustrating in Figure 4 the dangling bond concentration profile along the p-i-n device, at the annealed and final degraded states. As a result of the nonuniform light absorption, and then the non uniform generation rate, the light-induced increase in the dangling bond density occurs inhomogeneously along the device, as shown in the figure.

In Figure 5 the computed free electron and hole density profiles are plotted under the short circuit condition, at the annealed and degraded states. The obtained profiles reveal a sig-

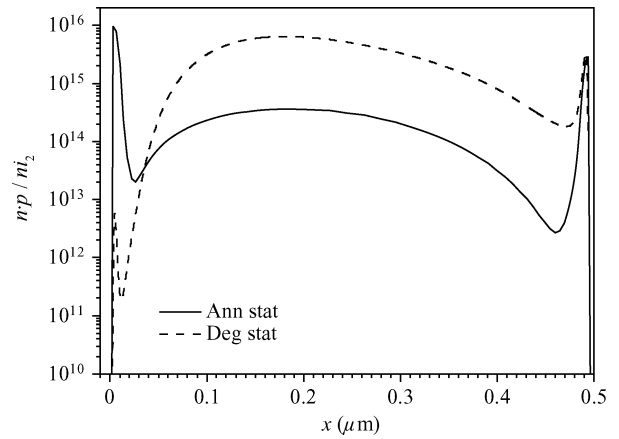


Figure 6. $n \cdot p$ product profile, under short circuit condition.

nificant difference between the free carrier populations in the two cases. In the first case, the free hole density dominates until $0.23 \mu\text{m}$. Afterwards, the free electrons become the dominating free charge carriers. In the degraded state an important decrease in hole density occurs around the p-i interface. This is obvious since the p-i defect density is nearly 4 times greater than that of the annealed state. Holes remain the dominating carriers but just until $0.07 \mu\text{m}$ when the electrons become the dominating free carriers for the remaining part of the device. Moreover, there is a considerable increase of electron and hole densities along the i-layer, which raises the $n \cdot p$ product nearly by 20 times compared to the annealed state, as shown in Figure 6. However, there is no further remarkable increase of the $n \cdot p$ product at the i-n interface while there is a noticeable decrease at the p-i interface which is due, as mentioned above, to the decrease of the hole density in this region.

Figures 7(a) and 7(b) show, respectively, the recombination rate and the trapped charge at the different gap states in the annealed state, while Figures 8(a) and 8(b) show those in the degraded one. In the first case (Figure 7(a)), the dominating recombination path until $0.11 \mu\text{m}$ is found in dangling bonds via D^+ (U_{db}^+), which are the recombination centres for electrons. In this region the electrons are captured in D^+ to produce D^0 . From 0.11 to $0.33 \mu\text{m}$ the recombination path via the valence band tail dominates (U_v), where the electrons are captured by the hole-occupied states. From $0.33 \mu\text{m}$ to the back of the device, the dominating recombination rate becomes via D^0 , here the electrons are captured in D^0 to produce D^- , which are recombination centres for holes in this area. With the assumption that the capture coefficients of the charged states of band tails and of dangling bonds are equals ($C_{ct} = C_{cd} = 10^{-7}$ cm³/s), the high recombination rate near the two interfaces is then due to the high hole density near the p-i interface and the high electron density near the i-n interface, which make Equations (1) and (2) the D^+ and D^- dominant, and (2) the $n \cdot p$ product significant, in these two regions, respectively, compared to the bulk of the i-layer.

Returning now to the trapped charge density (Figure 7(b)), we found that the dominating one in the front of the device is in D^+ . From 0.1 to $0.23 \mu\text{m}$, the charge trapped in the valence band tail contributes significantly in the positive charge which dominates in this region. Beyond $0.3 \mu\text{m}$, the D^- states take

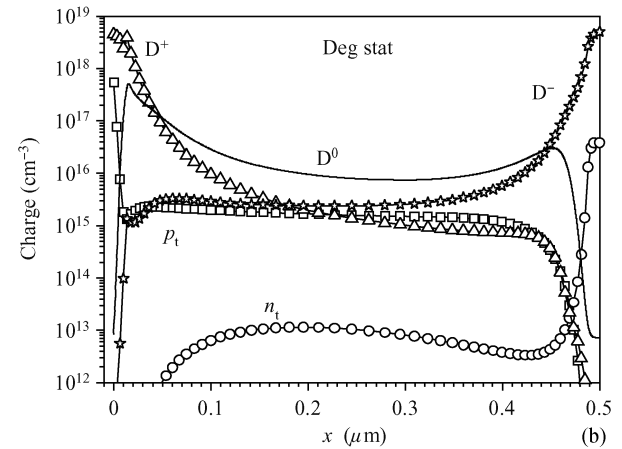
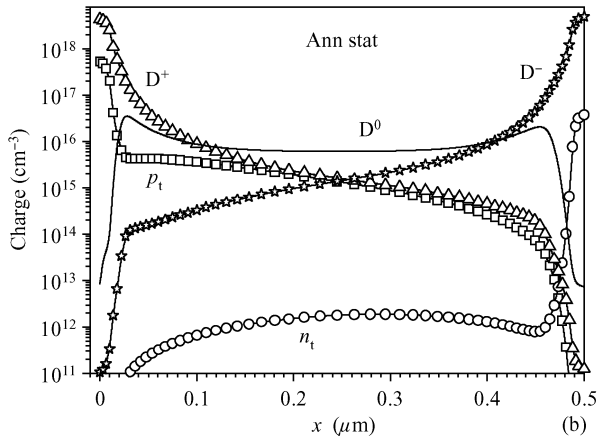
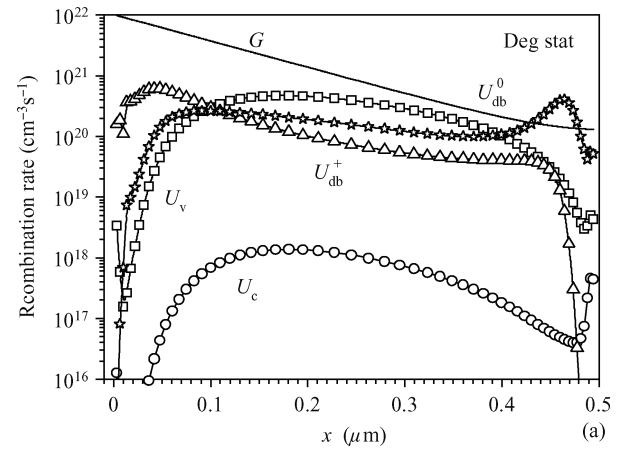
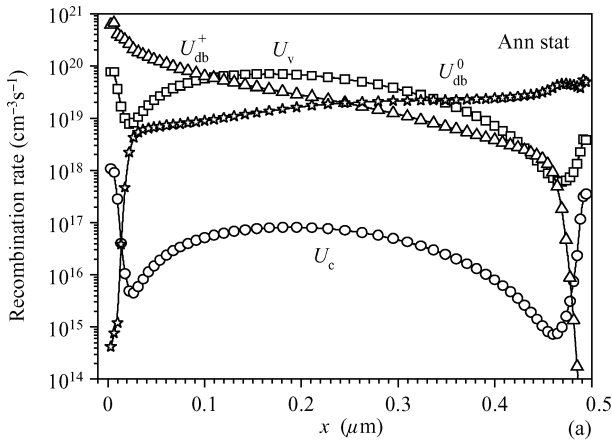


Figure 7. (a) Recombination rate profiles for tail bands, U_c , U_v and dangling bonds U_{db}^+ , U_{db}^0 , in annealed state. (b) Trapped charge density profiles in band tails, p_t , n_t , and dangling bonds D^+ , D^0 , D^- , in annealed state.

Figure 8. (a) Recombination rate profiles for tail bands, U_c , U_v and dangling bonds U_{db}^+ , U_{db}^0 , in degraded state. (b) Trapped charge density profiles in band tails, p_t , n_t , and dangling bonds D^+ , D^0 , D^- , in degraded state.

over as the dominating charge states, which forces the sign reversal.

In the degraded state (Figures 8(a) and 8(b)), we found an increase in all recombination rates which is caused mainly by the increase of the $n \cdot p$ product along the i-layer. At the p-i interface, where the highest D^+ defect density ($4 \times 10^{18} \text{ cm}^{-3}$) is located, there is no significant increase of the dominating recombination rate via D^+ , compared to the annealed state, due to the $n \cdot p$ product decrease. From the p-i interface to $0.04 \mu\text{m}$, an increase of the recombination rate via D^+ is found, which is caused by both the high D^+ density and the beginning of a considerable increase in the $n \cdot p$ product. However, beyond $0.04 \mu\text{m}$ this recombination rate decreases, therefore following the D^+ decrease, in spite of the increase of the product $n \cdot p$. From 0.1 to $0.4 \mu\text{m}$ the recombination rate dominates via the valence band tail, while from the last value to the back of the device, the dominating recombination rate path is found via D^0 . The latter exhibits a peak at $0.46 \mu\text{m}$, which is related to the D^0 peak at the same position (see Figure 8(b)).

We also see an increase in the D^- charge density (Figure 8(b)), which occurs from the p-i interface to $0.3 \mu\text{m}$. A similar effect is found for both valence band tail and D^+ charge densities in the region between 0.3 and $0.35 \mu\text{m}$. This means the appearance of a nearly neutralised region which is, from the figure, situated between 0.2 and $0.35 \mu\text{m}$. Here the D^- charge

density is compensated by the positive charge densities of the valence band tail and D^+ . This means the disappearance of the space charge in this region and a diminution of the electric field is therefore expected here.

It can be seen furthermore that the recombination rate via the conduction band tail, in the annealed and degraded states, is far lower in comparison to the recombination rate via the valence band tail and dangling bonds. Moreover, its spatial variation has a shape similar to the one of the $n \cdot p$ product variation, in the two cases. This is also obtained for the recombination rate via the valence band tail, which means that these recombination rates depend mainly on the $n \cdot p$ product, while the recombination rate via dangling bonds depends mainly on their density of states.

Figures 9–12 show, respectively, the band structure, the electric potential, the electric field and the space charge profiles, in both annealed and degraded states. From Figures 9(a) and 9(b), we see clearly that the light-induced defects cause an abrupt band bending near the p-i interface and consequently a low electric field in the i-layer, while a very high field at the p-i interface is expected. Indeed, these two points are revealed in Figures 10 and 11. As shown in Figure 10, the potential profile in the degraded state varies strongly around the p-i interface while it becomes nearly constant along the i-layer. Examining

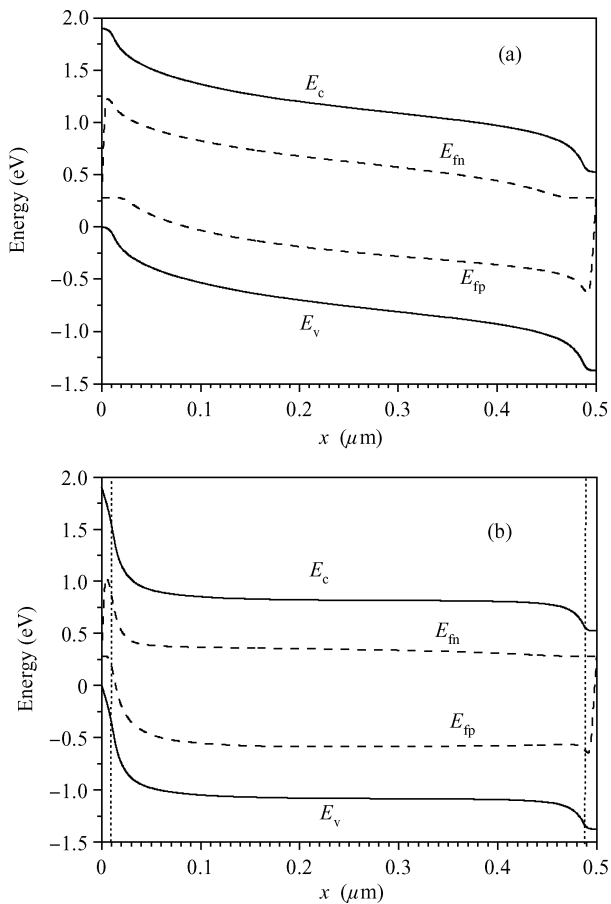


Figure 9. Gap structure under short circuit condition in (a) annealed state and (b) degraded state.

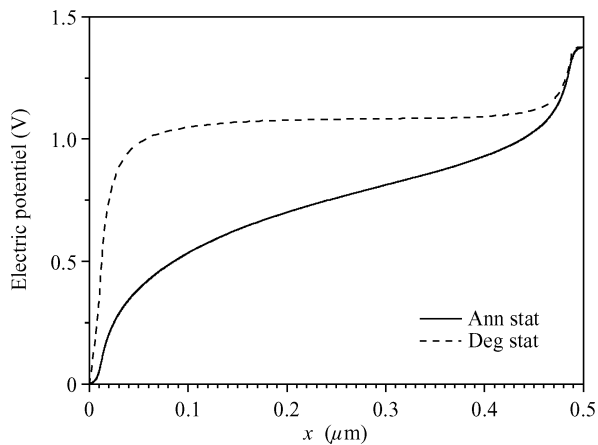


Figure 10. Electric potential profile, under short circuit condition.

Figure 11, showing the electric field profile, we see that the electric field increases from the edges of the device to the interfaces p-i and i-n, then it decreases towards the i-layer. The high interface fields are caused by large space charge densities in the p and n layers. For the annealed state, if one referred to Figure 12, we find that the depletion regions resulting from the p-i and i-n interfaces are overlapped in the i-layer. In the degraded state, a very high electric field is found indeed at the p-i interface as expected above, while it decays through the i-layer and reaches 300 V/cm at 0.3 μm. This means the sep-

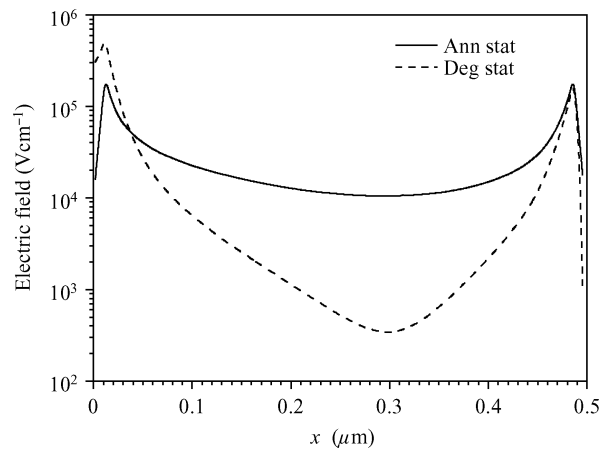


Figure 11. Electric field profile, under short circuit condition.

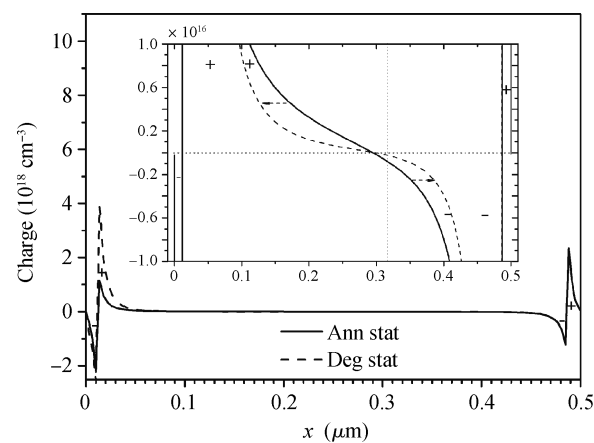


Figure 12. Space charge profile, under short circuit condition.

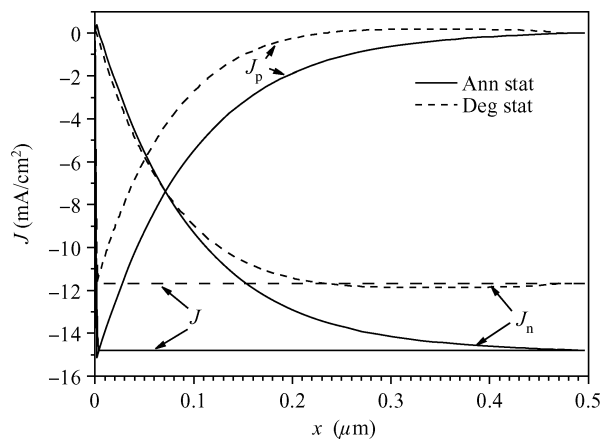


Figure 13. Electron and hole current density profiles.

aration of the depletion regions, and hence, the apparition of a nearly neutral region through which the electric field lowered. This is illustrated by Figure 12 and approves what has been advanced previously when one treated the trapped charge profiles in different gap states. As a result of this decrease in the electric field profile, additional recombination is induced through the i-layer, which was indeed found from the recombination rate profiles in the degraded state (Figure 8(b)).

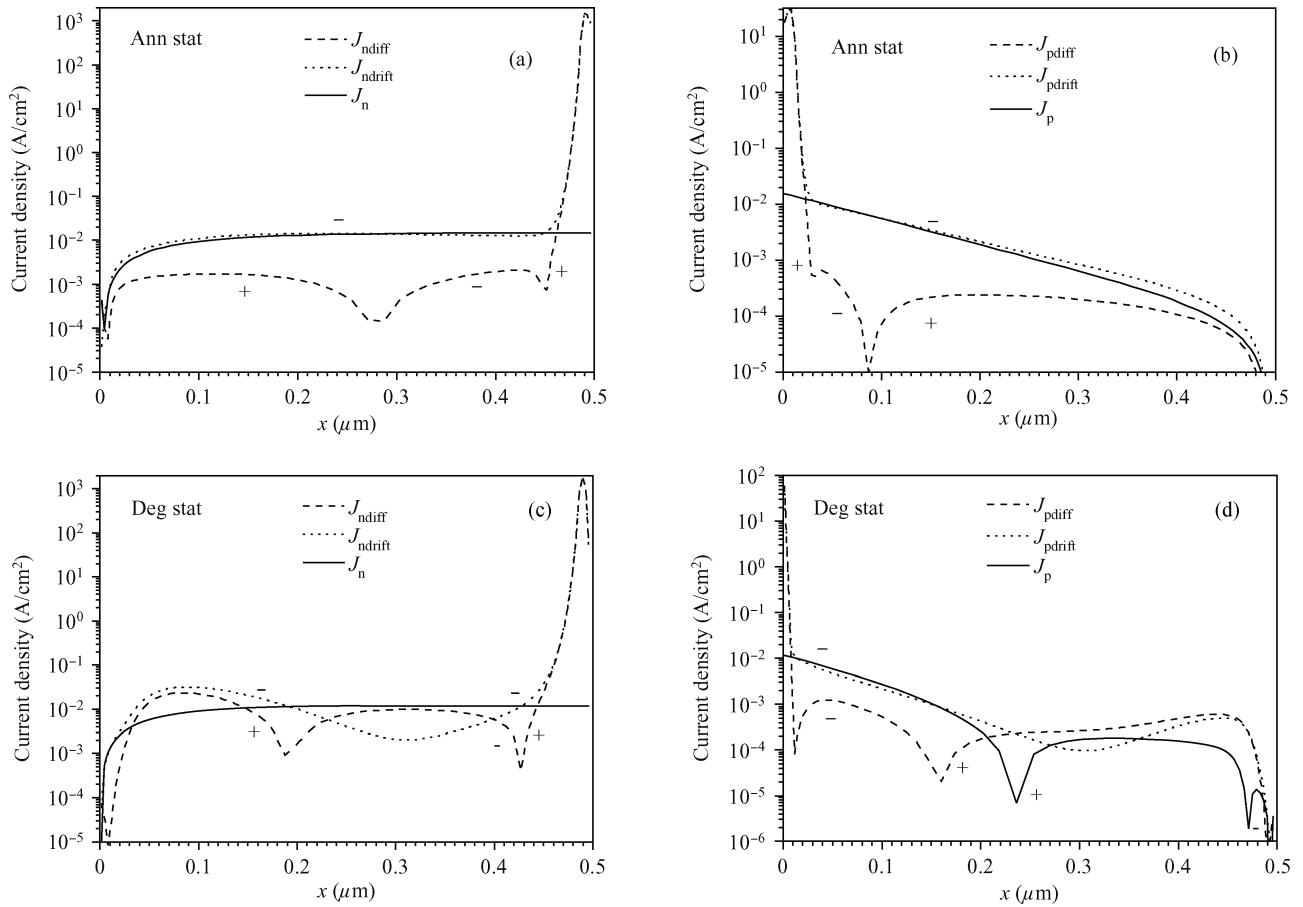


Figure 14. (a) Drift- and diffusion-electron current density profiles in annealed state. (b) Drift- and diffusion-hole current density profiles in annealed state. (c) Drift- and diffusion-electron current density profiles in degraded state. (d) Drift- and diffusion-hole current density profiles in degraded state.

Figure 13 shows electron, hole and total current density profiles calculated under short-circuit condition, at annealed and degraded states. A comparison of the electron current density and the hole current density, which are both negative, with the total current density shows that the current is mainly carried by electrons. Only in the region close to the p-i interface ($0.07 \mu\text{m}$ in the annealed state, $0.05 \mu\text{m}$ in the degraded one), where the hole concentration is much higher than the electron one, the hole current density provides the total current density. The degradation of the electron and the hole current densities is clearly shown and causes the decrease of the total current density from 14.75 to 11.68 mA/cm^2 . Moreover, we remark that there is a very weak decrease in both electron and hole current density profiles from $0.44 \mu\text{m}$ at the degraded state. This is explained by the recombination rate which locally exceeds the generation rate, as can be seen in Figure 8(a). In order to analyze in more detail the transport mechanism, in Figures 14(a)–14(d), electron and hole current densities are separated into drift and diffusion components. For both annealed and degraded states, the majority carrier current densities compete in drift and diffusion in the very front of the sample (close to the p-i interface) as in the back (close to the i-n interface). In the very front of the sample the dominating partial current densities are hole-drift and hole-diffusion current densities. These current densities nearly compensate each other but the drift current density exceeds the diffusion current density, so there are

different results in the total current density in this region. Similar results hold for electrons in the back of the device. We note here that an exception in the degraded state is found for holes at the p-i interface. Here there is a large decrease of free hole density, which are captured by the high D^+ density, compared to the annealed state (see Figure 5). Consequently, the hole-diffusion current density decreases significantly and the transport process remains drift-dominated in this region.

Along the i-layer, for electrons as for holes, the drift current density (negative) is the dominant partial current density in the annealed state, for which the electric field strength is high in the active region. However, the competition between the drift and diffusion current densities persists in the degraded state. The region where the diffusion current density dominates is here where the electric field is low, therefore weakening the drift current density.

In Figures 15 and 16 we present, respectively, the calculated current density J and the power density P provided by the cell, as a function of bias voltage under illumination; results are given for the annealed and the different degradation states. The degradation of the current density–voltage (J – V) and the power density–voltage (P – V) curves is clearly observed with an increasing number of dangling bonds, distributed inhomogeneously in the sample. In Figures 17(a)–17(d) we present the degradation effect on the cell photo-parameters; J_{sc} , V_{oc} , FF and P_{max} are plotted against the $N_d(t)/N_d(0)$ ratio. $N_d(t)$ is

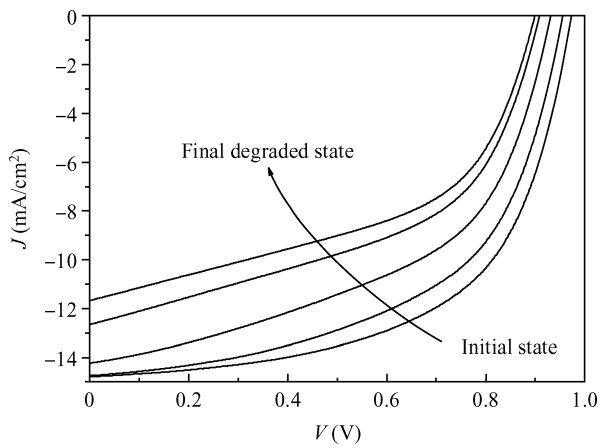


Figure 15. J - V characteristic degradation.

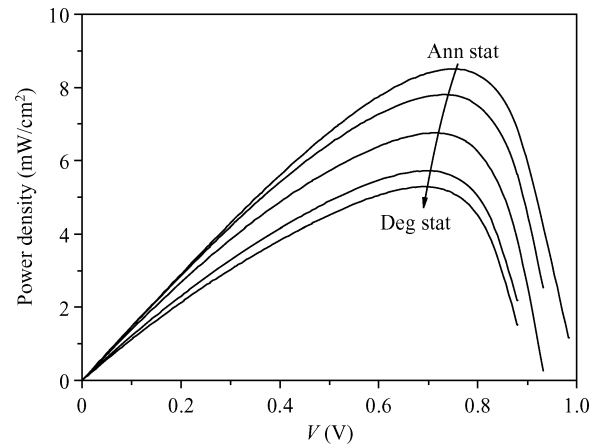


Figure 16. P - V characteristic degradation.

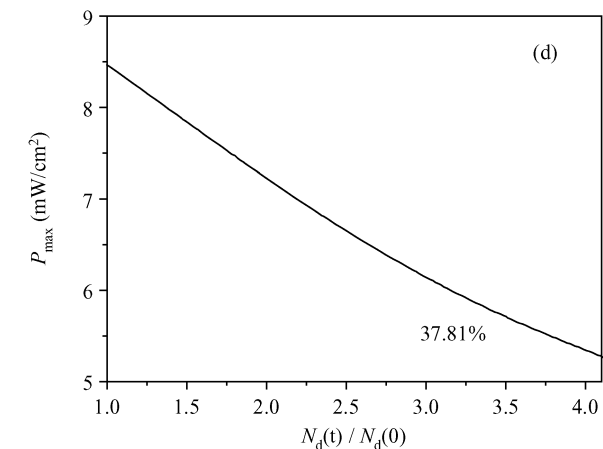
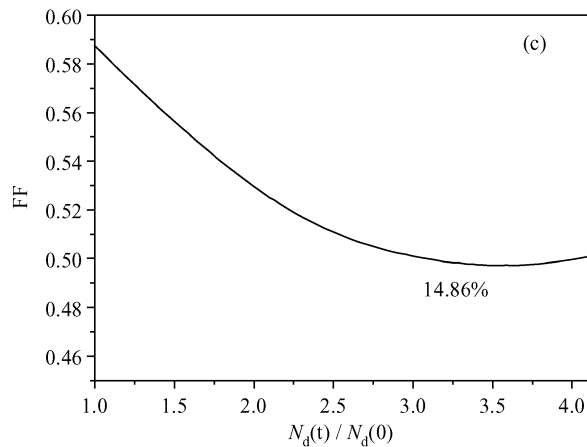
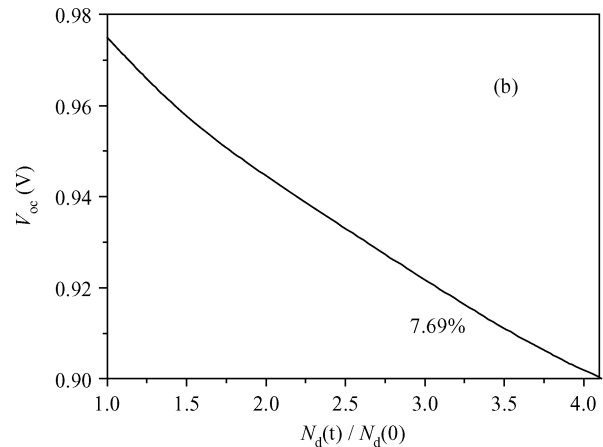
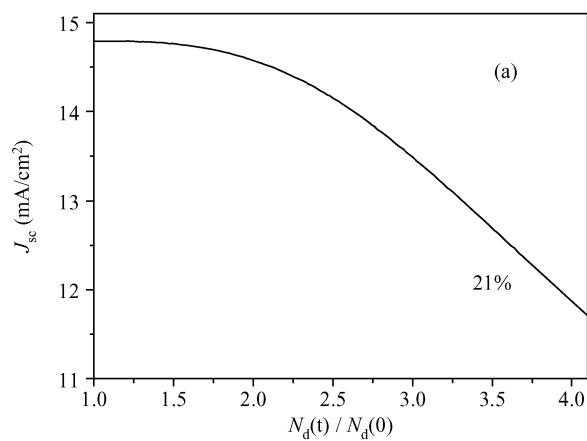


Figure 17. Cell photo-parameters versus $N_d(t)/N_d(0)$ ratio. (a) J_{sc} , (b) V_{oc} , (c) FF, and (d) P_{max} .

the dangling bond defect concentration in the sample at the different illumination times, t , and $N_d(0)$ is the initial (annealed) concentration of the dangling bonds. From these figures, J_{sc} exhibits a degradation of 21%, while V_{oc} decreases only by 7.69%, FF which is related to the curvature of the J - V characteristic shows a considerable degradation of 14.72% and P_{max} , which reflects the cell conversion efficiency, degrades by 37.81%. These results indicate that V_{oc} is the less sensitive parameter to the variation of the dangling bond density. However, P_{max} is the most affected parameter by degradation since

it depends on the maximum current density and the maximum voltage, which are both affected by degradation.

In Figures 18(a)–18(d) we plotted the solar cell performance parameters versus $N_d(t)/N_d(0)$, for μ_n between 10 and $25 \text{ cm}^2/(\text{V}\cdot\text{s})$, when $\mu_n/\mu_p = 10$, and for μ_n between 20 and $25 \text{ cm}^2/(\text{V}\cdot\text{s})$ when μ_p is raised to $6 \text{ cm}^2/(\text{V}\cdot\text{s})$. Here the aim is to examine the sensitivity of the J - V characteristic degradation to the free electron and hole mobilities. It is known that larger μ_n allows electrons to avoid holes in the bulk and be successfully collected. Thus the increase that is exhibited, J_{sc} , FF

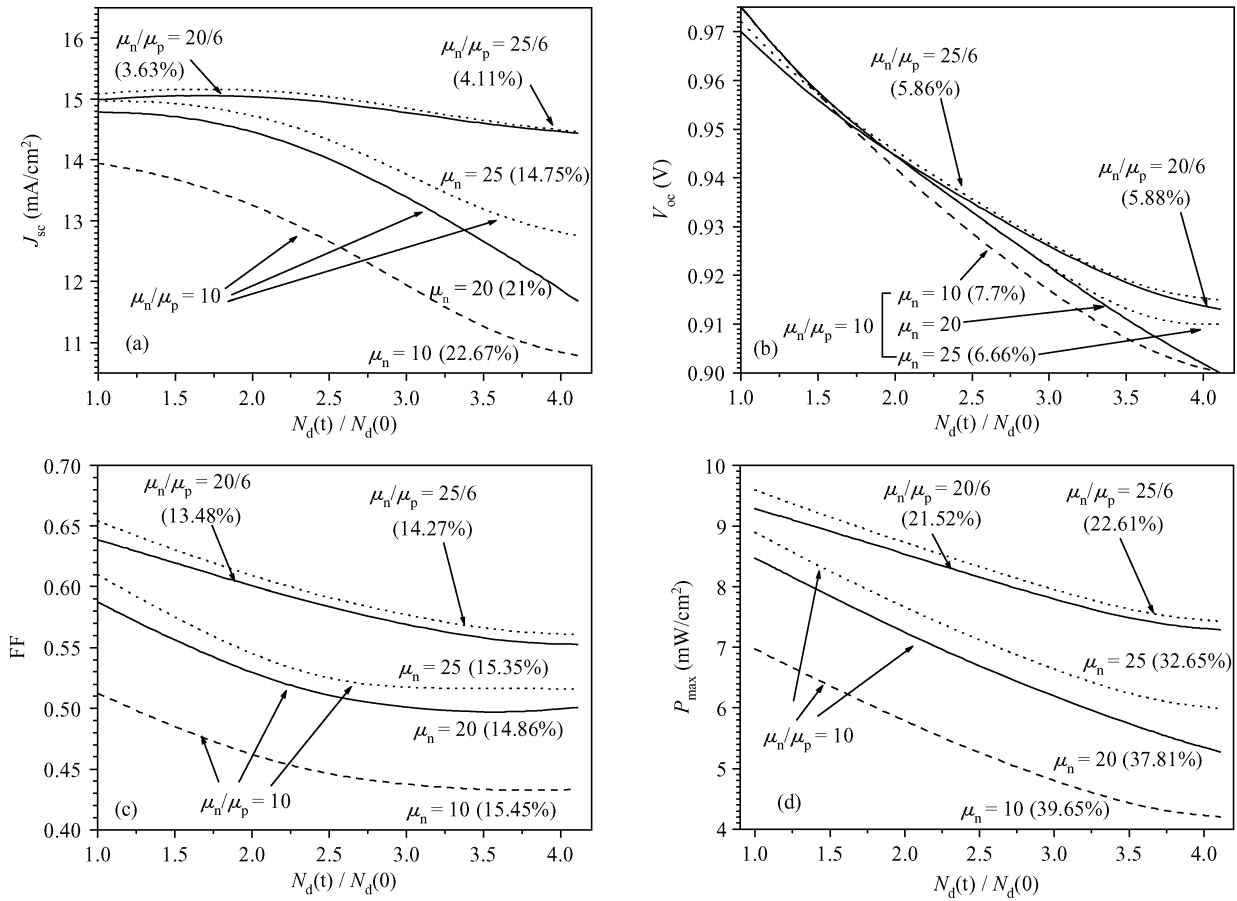


Figure 18. Influence of free electron and hole mobilities on degradation of (a) J_{sc} , (b) V_{oc} , (c) FF, and (d) P_{max} .

and P_{max} , in the annealed state as in the degraded one, means that these parameters depend on the efficiency with which electrons are collected. Moreover, except the FF degradation which changes weakly (14.86%–15.45%), we find that the J_{sc} degradation lowers from 22.67% for $\mu_n = 10$ cm²/(V·s) to 14.75% for $\mu_n = 25$ cm²/(V·s). A similar observation is found for P_{max} , which exhibits less degradation of 32.65% for $\mu_n = 25$ cm²/(V·s) in front of 39.65% for $\mu_n = 10$ cm²/(V·s). However, V_{oc} is nearly insensate to μ_n , especially in the annealed state. Nevertheless it undergoes less degradation (6.66%) for $\mu_n = 25$ cm²/(V·s).

For the actual case since $\mu_n/\mu_p = 10$, μ_p varies between 1 and 2.5 cm²/(V·s). These low values of μ_p imply a large availability of holes, which governs bulk recombination. The increase of μ_p to just 6 cm²/(V·s) has a significant influence on the cell parameter degradation, as it is shown in the same figures. In the annealed state, we can see that J_{sc} and V_{oc} exhibit a slight variation with increasing μ_p to 6 cm²/(V·s); J_{sc} increases only by 0.1–0.2 mA/cm² for $\mu_n = 20$ –25 cm²/Vs, while V_{oc} decreases by 4–5 mV, instead of increasing like the other parameters. In the degraded state, J_{sc} shows a degradation of 3.63%–4.11%, which is much lower than that obtained for $\mu_n/\mu_p = 10$ (14.75%–22.67%). The V_{oc} degradation percentage, however, decreases slightly from 7.7%–6.6% for $\mu_n/\mu_p = 10$ to 5.86%–5.88% for the actual case.

FF and P_{max} exhibit an appreciable dependency on μ_p , in the annealed state as in the degraded one. The FF degradation percentage decreases slightly with μ_n/μ_p ratio diminution

while P_{max} exhibits less degradation of 21.52%–22.61%.

These observations prove the fact that the free hole mobility has a more important impact on the reduction of the cell parameter degradation than that of electrons. By increasing μ_p from 2.5 to just 6 cm²/(V·s) the degradation that P_{max} (which reflects cell efficiency) undergoes decreases from ~ 33% to ~ 22%. However, V_{oc} is the less affected parameter by the μ_n increase or μ_n/μ_p ratio diminution. These two results concerning the crucial role of μ_p on the cell performance and the unobvious relation between V_{oc} and the cell efficiency improvement are in agreement with what was pointed out by Chatterjee^[18] and Dutta *et al.*^[19], respectively.

6. Conclusion

Our model of the light-induced defect creation together with the numerical modelling of the a-Si:H p–i–n solar cell have been used to provide the physical mechanisms governing the operation of the device under illumination and its degradation effect. In this approach, we have considered the simple case of a monochromatic light beam nonuniformly absorbed and the reason why the generation rate decreases exponentially from the illuminated p-side to the n-side of the device. We have interpreted our results on the basis of an inhomogeneous increase of the dangling bond defect distribution, as a consequence of the degradation effect related to the absorbed light profile in the i-layer. The effect of this distribution is concretised by showing the induced changes in the internal variable profiles through the device and in its external photo-

parameters. These changes are summarised as follows:

(1) An important increase in recombination rate, due mainly to the increase of the bulk $n \cdot p$ product, the reason why the current density decreases considerably along the device.

(2) An abrupt band bending through the p-side and consequently a high electric field in this region, while a low electric field is found in the i-layer. The latter further encourage the bulk recombination of free carriers.

(3) The carrier diffusion current densities across the i-layer, neglected in the annealed state, contribute significantly to the total current density (mainly the electron diffusion current density).

(4) Decreases occur in the photo-parameters, which can be concretised in terms of percentages: 21% in J_{sc} , 7.69% in V_{oc} , 14.86% in FF and 37.81% in P_{max} , for the case of $\mu_n = 20 \text{ cm}^2/(\text{V}\cdot\text{s})$ where $\mu_n/\mu_p = 10$. P_{max} is the most affected parameter by degradation while V_{oc} is the less affected one. Increasing the free electron mobility to $25 \text{ cm}^2/(\text{V}\cdot\text{s})$ improves the solar cell performance, since it causes a considerable diminution in the degradation percentages, especially that of P_{max} which decreases to $\sim 33\%$. Furthermore, increasing μ_p to just $6 \text{ cm}^2/(\text{V}\cdot\text{s})$ reduces, in a more significant way, the degradation percentage of P_{max} from 33% to 22%. Finally, the very weak sensitivity that exhibits V_{oc} to the free carrier mobilities led us to conclude that the relation between V_{oc} and the cell efficiency improvement is not obvious.

References

- [1] Staebler D L, Wronski C R. Reversible conductivity changes in discharge-produced amorphous Si. *Appl Phys Lett*, 1977, 31: 292
- [2] Stutzmann M, Jackson W B, Tsai C C. Light-induced metastable defects in hydrogenated amorphous silicon: a systematic study. *Phys Rev B*, 1985, 32: 23
- [3] Meftah A F, Meftah A M, Merazga A. A theoretical study of light induced defect creation, annealing and photoconductivity degradation in a-Si:H. *J Phys: Condens Matter*, 2004, 16: 3107
- [4] Meftah A F, Meftah A M, Merazga A. Modelling of Staebler-Wronski effect in hydrogenated amorphous silicon under moderate and intense illumination. *Defect and Diffusion Forum*, 2004, 230–232: 221
- [5] Powell M J, Wehrspohn R B, Deane S C. Nature of metastable and stable dangling bond defects in hydrogenated amorphous silicon. *J Non-Cryst Solids*, 2002, 299–302: 556
- [6] Han D. Search for the factors determining the photodegradation in high efficiency a-Si:H solar cells. Report, March 2002, NREL/SR-520-31754
- [7] Cheong H M, Lee S H, Nelson B P, et al. Light-induced long-range hydrogen motion in hydrogenated amorphous silicon at room temperature. *Appl Phys Lett*, 2000, 77: 2686
- [8] Branz H M. Hydrogen collision model of light-induced metastability in hydrogenated amorphous silicon. *J Solid State Commun*, 1997, 105: 387
- [9] Godet C. Metastable hydrogen atom trapping in hydrogenated amorphous silicon films: a microscopic model for metastable defect creation. *Philos Mag B*, 1998, 77: 765
- [10] Biswas R, Pan B C. Defect kinetics in new model of metastability in a-Si:H. *J Non-Cryst Solids*, 2002, 299–302: 507
- [11] Morigaki K, Hikita H. Model of the light-induced creation of two types of dangling bonds in a-Si:H. *J Non-Cryst Solids*, 2000, 266–269: 410
- [12] Aida M S, Youla F, Touefek N, et al. Light induced defects in sputtered amorphous silicon thin films. *Mate Chem Phys*, 2002, 74: 251
- [13] Powell M J, Deane S C. Defect-pool model and the hydrogen density of states in hydrogenated amorphous silicon. *Phys Rev B*, 1996, 53: 10121
- [14] Powell M J, Deane S C. Improved defect-pool model for charged defects in amorphous silicon. *Phys Rev B*, 1993, 48: 10815
- [15] Schmidt J A, Arce R, Buitrago R H, et al. Light-induced defects in hydrogenated amorphous silicon studied by the constant-photocurrent method. *Phys Rev B*, 1997, 55: 9621
- [16] Schmidt J A, Arce R D, Koropecski R R, et al. Light-induced creation of metastable defects in hydrogenated amorphous silicon studied by computer simulations of constant photocurrent measurements. *Phys Rev B*, 1999, 59: 4568
- [17] Meftah A M, Meftah A F, Hiouani F, et al. Numerical simulation of the defect density influence on the steady state response of a silicon-based p–i–n cell. *J Phys: Condens Matter*, 2004, 16: 2003
- [18] Chatterjee P. Photovoltaic performance of a-Si:H homojunction solar cells: a computer simulation study. *J Appl Phys*, 1994, 76(2): 1301
- [19] Dutta U, Chatterjee P. The open-circuit voltage in amorphous silicon p–i–n solar cells and its relationship to material, device and dark diode parameters. *J Appl Phys*, 2004, 96(4): 2261